AGU PUBLICATIONS

Geophysical Research Letters

RESEARCH LETTER
10.1002/2013GL057928

Key Points:
- New algorithms are used to identify regions containing isochronous reflectors
- The data set contains 36% isochronous reflector across ~200,000 km of flight line
- Isochronous data are more common inland and where less cold glacial ice occurs

Supporting Information:
- Readme
- Text S1

Correspondence to:
L. C. Sime,
lsim@bas.ac.uk

Citation:
Sime, L. C., N. B. Karlsson, J. D. Paden, and S. Prasad Gogineni (2014), Isochronous information in a Greenland ice sheet radio echo sounding data set, *Geophys. Res. Lett.*, *41*, 1593–1599, doi:10.1002/2013GL057928.

Received 6 SEP 2013
Accepted 11 FEB 2014
Accepted article online 14 FEB 2014
Published online 5 MAR 2014

Isochronous information in a Greenland ice sheet radio echo sounding data set

Louise C. Sime[1], Nanna B. Karlsson[2], John D. Paden[3], and S. Prasad Gogineni[3]

[1]British Antarctic Survey, Cambridge, UK, [2]Centre for Ice and Climate, Niels Bohr Institute, University of Copenhagen, Copenhagen, Denmark, [3]Center for Remote Sensing of Ice Sheets, Lawrence, Kansas, USA

Abstract The evaluation of ice sheet models is one of the pressing problems in the study of ice sheet dynamics. Here we examine the question of how much isochronous information is contained within the publicly available Center for Remote Sensing of Ice Sheets (CReSIS) Greenland airborne radio echo soundings data set. We identify regions containing isochronous reflectors using automatic radio echo sounding processing (ARESP) algorithms. We find that isochronous reflectors are present within 36% of the CReSIS radio echo sounding englacial data by location and 41% by total number of data. Between 1000 and 3000 m in depth, isochronous reflectors are present along more than 50% of the data set flight path. Lower volumes of cold glacial period ice also correspond with more isochronous reflectors. We find good agreement between ARESP and continuity index results, providing confidence in these findings. Ice structure data sets, based on data identified here, will be of use in evaluating ice sheet simulations and the assessment of past rates of snow accumulation.

1. Introduction

The evaluation of ice sheet models is an urgent problem both with respect to sea level forecasting and the understanding of ice sheet dynamics. The Greenland polar ice sheet is the second largest ice body in the world. It contains about 2.85 million km^3 of ice, equivalent to a global sea level rise of 7.2 m. Change in the Greenland ice sheet volume will directly affect Atlantic circulation, climate, and global sea level. Models of Greenland ice flow dynamics are at a stage where the resultant estimates of sea level change are consistent with available observations. Even so, the Fifth Assessment Report Intergovernmental Panel on Climate Change places sea level change estimates at only a medium confidence level, partly because observations of large-scale ice flow dynamics remain short [*Intergovernmental Panel on Climate Change*, 2013]. Improving our understanding of the nature of the Greenland ice sheet, and its ice flow, is thus an urgent problem [e.g., *Velicogna*, 2009].

Difficulties in ice sheet model evaluation stem partly from a lack of available data sets that quantify the internal structure of the ice sheets. This problem can potentially be addressed using observed ages of the ice [*Clarke et al.*, 2005; *Lhomme et al.*, 2005]; however, such studies have generally been restricted to using observations from sparse ice core data sets. If larger amounts of age data are available, however, such data set could be used to spin up and to test models [e.g., *Heimbach and Bugnion*, 2009; *Hindmarsh et al.*, 2009; *Leysinger Vieli et al.*, 2011]. For this reason, ice sheet and consequent sea level predictions may stand to gain from the automatic acquisition of ice sheet scale data sets [*Sime et al.*, 2011; *Karlsson et al.*, 2012]. Quantifying the isochronous information present in airborne radio echo sounding geophysical surveys is likely the best available route toward achieving this goal.

Airborne radio echo sounding (RES) systems operate by emitting a radar pulse which propagates through the air and the ice sheet. Energy from the pulse is reflected at boundaries between materials of differing dielectric properties, and the return signal is recorded. Continuous internal ice reflectors are usually thought to be isochronous [*Bogorodsky et al.*, 1985; *Eisen*, 2008]. RES observations can therefore provide information about the englacial age structure [e.g., *Fahnestock et al.*, 2001; *Eisen*, 2008; *Matsuoka et al.*, 2009] and ice flow conditions [*Leysinger Vieli et al.*, 2007; *Karlsson et al.*, 2012].

There has been recent progress made in terms of automatically quantifying the amount and type of englacial ice structure information within polar ice sheet RES data. RES echo strength data are typically presented in two formats: as a plot of each trace, sometimes referred to as an A-scope, and as an image

comprising a series of adjacent traces, sometimes referred to as a Z-scope. Making use of A-scope profiles, *Karlsson et al.* [2012] approached the problem of automatic quantification by developing an algorithm to examine the degree of reflector continuity. They find that their continuity index corresponds closely with ice flow speed. An alternative approach is outlined in *Sime et al.* [2011]. The automatic RES processing (ARESP) method of *Sime et al.* [2011] uses RES binary images, each derived from original Z-scopes, to enable characterization of reflectors. Here we further develop and apply the *Sime et al.* [2011] quantification method based on image processing, we present the first ice sheet scale application of the method, and we compare results to those derived using the *Karlsson et al.* [2012] approach. This allows us to estimate the total amount of recoverable isochronous information from the Greenland Center for Remote Sensing of Ice Sheets (CReSIS) RES data set. The work describes how new approaches might help the evaluation of ice sheet simulations, by enabling ice sheet modelers to understand the amount of information which can automatically derived from existing radio echo sounding data sets.

2. Data and Methods

2.1. The CReSIS Greenland RES Data Set

The Center for Remote Sensing of Ice Sheets (CReSIS; University of Kansas) Greenland data set has been acquired over a period of 19 years, using an evolving series of radar systems and airborne platforms [*Namburi*, 2003; *Lohoefener*, 2006; *Namburi*, 2007; *Gogineni et al.*, 2007; *Oswald and Gogineni*, 2008]. While studies using the CReSIS RES data have tended to focus on basal topography [*Gogineni et al.*, 2001], the radar depth sounder measurements feature extensive isochronous internal layering [e.g., *Fahnestock et al.*, 2001; *Gogineni et al.*, 2007]. These observable englacial reflectors are present within a significant, but presently unknown, proportion of the retrieved RES observations. They provide the potential for the recovery of englacial ice structure data from within a few hundred meters of the ice surface to within a few hundred meters of the bed.

CReSIS data used here were downloaded on 15 July 2013 from https://data.cresis.ku.edu/data/rds/ [*Gogineni*, 2012], a total of 18,836 files. CReSIS flight lines extend across the whole of Greenland (Figure 1a). CReSIS in-house processing tends to generate three files for most flight segments. The first file is formed from data with low-gain settings for the air-ice interface and upper-ice layers retrieval, the second file is formed from data with high-gain settings for the ice bottom interface and deep ice layer retrieval, and the third file is a combined product. Here on advice from the CReSIS team, we use the combined file product, which is combined at a fixed time after the surface return. In practice, this means excluding any individual high- or low-gain files, which excludes 11,399 files. Any radar returns that were within-air or within-bedrock (above or below the ice) are also discarded. This is achieved using the ice bottom and ice surface location information included with the CReSIS files. Flight segments where ice bottom and ice surface could not be located, or which featured less than 100 englacial echoes were also discarded, resulting in a further 683 file discards. A total of 6753 files contain enough englacial data to be processed, themselves extracted from across 19 flight campaigns, along 393,953 km of flight path. A full breakdown of data by year, radar system, and air platform is provided in Appendix A.

2.2. The ARESP Algorithm

The ARESP algorithm uses feature recognition to assess the likelihood that binary Z-scope images contain isochronous reflectors. Rather than tracing a single layer across the CReSIS data set, the basic results from the *Sime et al.* [2011] method are reflector dip angles across each individual flight segment. If these dip angles are horizontally integrated, the resultant product is equivalent to tracing layers across the segments. The slope and number of englacial reflectors are measured over very short lengths: tens of meters. This approach of using a binary "layer" or "not-layer" version of the Z-scopes is computationally efficient [e.g., *Sime and Ferguson*, 2003]. Additional properties of the identified short layer binary objects also help enable classification of each reflector object. ARESP can thus be used to assess the likelihood that each automatically measured object represents a reflection of an isochronous feature.

Binary versions of the Z-scope images are separated into thin (vertical) strips. Properties of the layer "objects," isolated through this process, are measured. These properties include the following: position, area, major axis length, minor axis length, and slope (or dip, or orientation). Any object that is too small, too large, or with an aspect ratio of less than three to one is eliminated, since these are very unlikely to represent true isochronous reflector objects [cf. *Sime et al.*, 2011]. In addition to these criteria which eliminate individual objects which are unlikely to be isochronous, we also examine the characteristics of very localized groups of

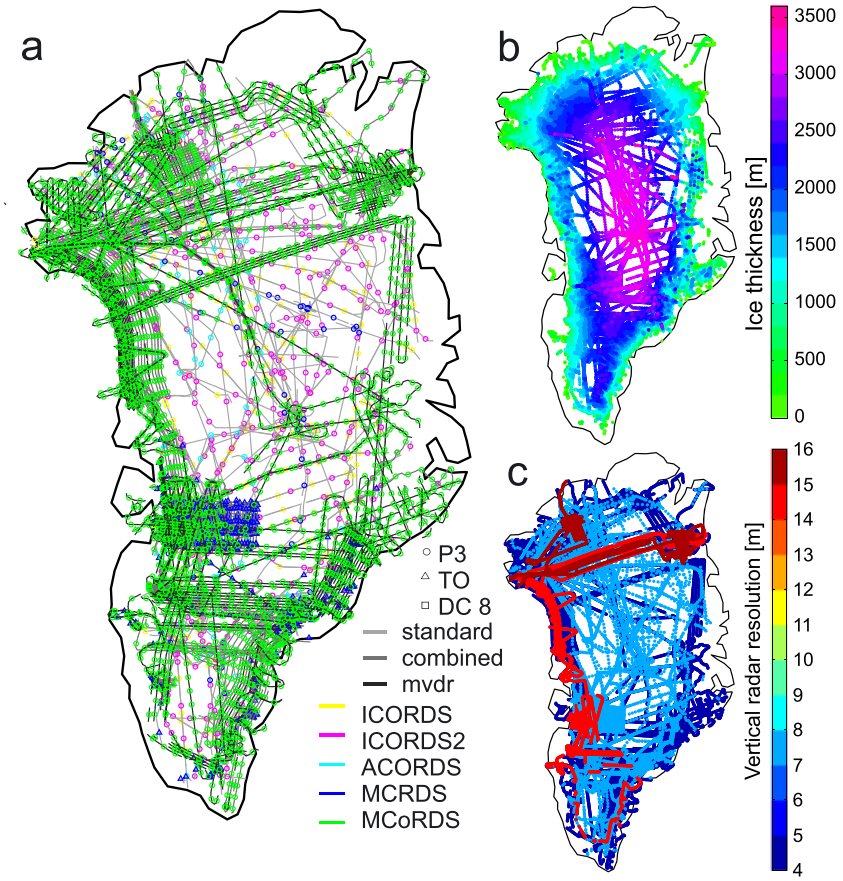

Figure 1. (a) A map of CReSIS radar echo sounding (RES) flight paths over Greenland. Data are classified by radar system (symbol colors); RES line quality (line gray scale); and airplane platform, where P3 is a Lockheed P-3 Orion, TO is a Twin Otter, and DC8 is a Douglas DC-8 (symbol type). (b) Ice thickness measurements from the CReSIS data set. Both the ice surface and ice bottom were either hand picked or automatically picked by the CReSIS team. (c) The RES vertical resolution (m). Resolution remains constant along each flight line.

objects. These groups, or populations, each comprises 100 or less objects within 250 m (approximate), in the vertical and horizontal directions, of the population center. For each of these local object populations, an actual number of objects, and variability of the object slopes, are then used to calculate whether RES data at this location are locally traceable isochronous reflectors. See *Sime et al.* [2011] for further details of the algorithms, and Appendix B for a discussion of the specific number of objects, and variability of the object slopes, threshold values.

2.3. The "Continuity Index" Algorithm

The continuity index algorithm is based on the observation that isochronous reflectors are represented in A-scope profiles as peaks of high reflected relative power bounded by lower values. A-scopes from regions of ice with many reflectors may thus exhibit high-amplitude fluctuations, while regions where these reflectors are less clear display fewer peaks in the A-scope profiles. The main difference between the two cases is therefore the rapidity with which the signal changes between extreme values. We can quantify this by using the absolute value of the gradient of the A-scopes, and this is what is referred to as the continuity index. Thus, areas with clear reflectors return a high continuity index, while areas where the reflectors are less clear or absent have a low continuity index. To help ensure the measured reflector continuity regionally representative, the calculated continuity index value is averaged over windows containing 100 A-scopes. For a more complete description of the algorithm, please see *Karlsson et al.* [2012].

3. Results

3.1. A Comparison of ARESP and Continuity Index Results

Continuity index results (Figure 2a) indicate extensive, continuous isochronous reflectors (high continuity index) in the central part of the ice sheet, while faster-flowing shallow areas have a low continuity index

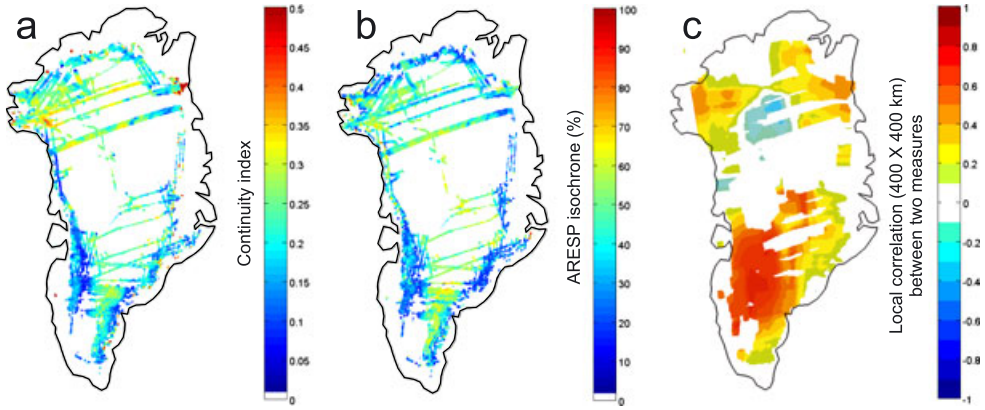

Figure 2. Comparison between (a) the continuity index and (b) the ARESP-based isochrone percentage estimate. Here we use only RES data from 2010 onward, obtained from a P3 aircraft platform. This is due to sensitivity of the continuity index to aircraft platform. All data is shown at 5 × 5 km resolution. (c) The local correlation between the two measures, calculated using a spatial sample of area 400 × 400 km. Each correlation value is calculated using available data (from Figures 2a and 2b) within 200 km of the mapped data point. The correlation calculation sample size in central regions is low compared with the more data-rich southern, northern, and coastal areas. Regions which have no data within 25 km of the grid point center are also masked.

(Figure 1b), indicating disrupted or absent isochrones. There are a few anomalously high data points along the margin of the ice sheet, which can be due to crevassing and the effect of ice close to the melting point, which can both occur where shearing or surface melting are present. The algorithm can misinterpret these phenomena as layering. ARESP results (Figure 2b) suggest a similar pattern, but with lower values over northeastern regions.

Comparing the continuity index and the ARESP-based isochrone percentage estimates at the 400 × 400 km regional scale, by calculating the correlation between the two measures within these regions, indicates that in central northern Greenland, the correlation between the two approaches is weak (Figure 2c). This could be partly due to less spatial variability (a much lower signal-to-noise ratio in ice flow speed) at the regional 400 km resolution. However, at the ice sheet scale, results from each algorithm tend to confirm the results of the other. This is despite their being based on independent data set quantities. A consequence of this similarity in results is the confidence it lends to ARESP-based estimates of the amount of isochronous information in the data set.

3.2. What Fraction of the Total Ice Depth Under Each Point on the Surface is Composed of Isochronous Reflectors?

The fraction of the total ice depth under each point on the surface is composed of isochronous reflectors, can be determined by calculating the fraction of the total ice depth under each point on the surface is filled with ARESP objects which possess consistent slopes, and which also have other quantities consistent with isochronous reflectors, as outlined in section 2.

Using ARESP measurements from across the whole data set there are two main possible approaches that could be used to define the quantity of "consistent reflector slopes." The first approach would use the assumption that measurable isochronous reflectors have variable slope properties across the data set. The second alternative assumption is that isochronous reflectors slopes possess similar characteristics throughout the data set. In the first case, the fundamental assumption is that the variance of the reflector slopes depends on the absolute local isochrone slope, while in the second case, the assumption is that these quantities are independent. In practice, using either assumption, the geographical pattern of isochronous reflectors remains similar (not shown) although the total estimated proportion of isochronous information somewhat depends on local threshold specification. It is possible to make a case for either scenario. However, based on observed CReSIS RES measurement noise patterns, we believe that the second scenario is probably more accurate for this data set. (From another viewpoint, this is also equivalent to assuming that nonisochronous reflector noise across the data set is uniform.) The implication of using the second assumption is that the estimation of the fraction of RES data which features measurable isochronous reflectors

Table 1. Total Distance of Reflectance Data and Isochronous Data by Depth

Depth (m)	Total (km '000s)	Isochronous (km '000s)	Isochronous (%)
250	305	67	22
500	313	75	24
750	305	109	36
1000	291	143	49
1250	276	154	56
1500	260	148	57
1750	239	137	57
2000	218	121	56
2250	196	107	55
2500	173	94	54
2750	153	81	53
3000	135	65	48
3250	118	53	45
3500	102	43	42

can be achieved using a single uniform threshold for the number of slope measurements, and the local variability of slope measurements, across the data set.

Using the principle of a uniform threshold (see Appendix B for threshold details), and when averaged across all flight segments, the total percentage of data containing isochronous reflectors is 35.6%. These isochronous reflectors are distributed throughout about 90% of our flight segments. Alternatively, if calculations are based on the total number of data, 41% of the data contain measurable isochronous reflectors. Isochronous reflectors occur more reliably within thicker inland ice. Between about 1000 and 3000 m in depth, isochronous reflectors typically occur over more than 50% of the flight path (Table 1). The occurrence of isochronous reflectors is mainly independent of radar system, aircraft platform, and year flown (Table 2).

3.3. What Ice Sheet Properties Determine the Occurrence of Isochronous Reflectors?

In terms of explaining the regional-scale patterns, the lower amount of isochronous data detected by ARESP in central north-east Greenland is likely due to cold ice, from the last glacial period (before approximately 21,000 years ago). In this region cold glacial period ice makes up a large percentage of the ice column [*Karlsson et al.*, 2013]. This cold glacial period ice has few traceable isochronous reflectors; thus, ARESP calculates a lower percentage of isochronous data in this region. Additionally, large basal ice features are observed in the region and these phenomena can show up as nonisochronous reflecting features. The processes behind their formation are not well understood but sticky and slippery spots, as well as basal accretion have been suggested [*Bell et al.*, 2011].

To the east, toward the coast, the percentage of reflectors that are isochronous rises. Here the transition to the colder glacial period ice occurs relatively deeper within the ice. The highest percentages, which are found in the western central region, are likely by a combination of low velocities (less disruption) paired with relatively less cold glacial period ice.

In addition to the north versus south patterns, less isochronous data occurs around the coast, particularly in southern and eastern regions. These regions, with low levels of isochronous data, tend to coincide with faster ice flow [*Joughin et al.*, 2010]. [*Karlsson et al.* 2012] note that reflector continuity decreases in the presence of fast flow. This flow speed explanation is backed up by the pattern of variance of the local reflector slopes (Figure 3c). Central and northern portions of the ice sheet tend to feature much lower slope variance values. This suggests that, within this slow moving ice, more of the reflectors tend to slope in the same direction. Within some coastal regions that feature faster flow, we see much higher values for the reflector slope variance. Additionally, isochronous reflectors generally cannot be identified in thin ice; reflected signals from internal layers in thin ice are often masked off-vertical rough-surface scatter. Since coastal ice also tends to be thinner, this also acts to reduce the amount of isochronous data.

Table 2. Percentage of Data That Are Isochronous

Year	Radar System	Air Platform	Data Type	Isochronous (%)
1993	ICORDS	P3	standard	46
1995	ICORDS	P3	standard	62
1996	ICORDS	P3	standard	66
1997	ICORDS	P3	standard	55
1998	ICORDS2	P3	standard	54
1999	ICORDS2	P3	standard	55
2001	ICORDS2	P3	standard	57
2002	ICORDS2	P3	standard	59
2003	ACORDS	P3	standard	46
2005	ACORDS	TO	standard	30
2006	MCRDS	TO	standard	56
2007	MCRDS	P3	standard	50
2008	MCRDS	TO	combined	29
2009	MCRDS	TO	mvdr	10
2010	MCoRDS	DC8	mvdr	41
2010	MCoRDS	P3	mvdr	26
2011	MCoRDS	P3	combined	41
2011	MCoRDS	TO	combined	20
2012	MCoRDS	P3	mvdr	41

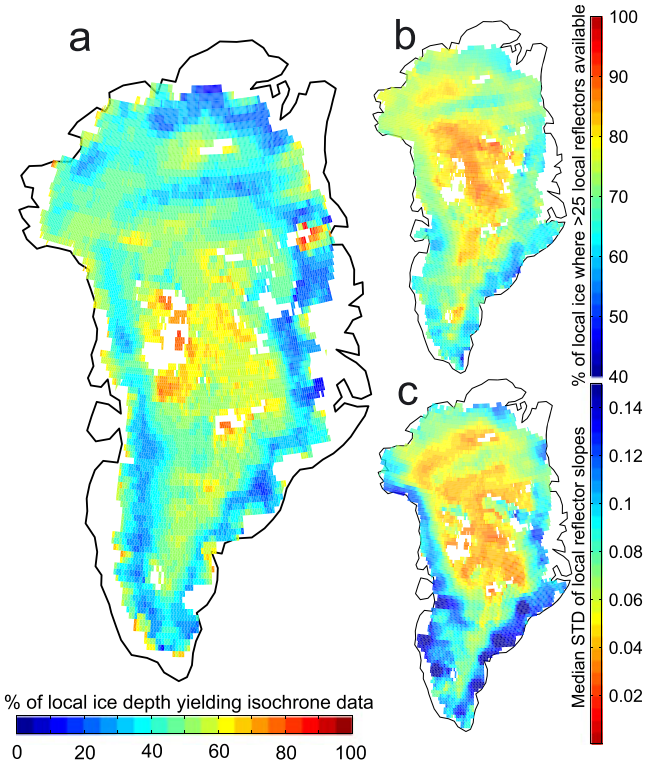

Figure 3. (a) Percentage of RES data that contain measurable isochronous reflectors, specifically the percentage of the local ice depth column which yields isochrone data. (b) The percentage of RES data where sufficient reflectors exist to enable statistically significant dip measurements. See Appendix B for further details. (c) Variance (median standard deviation) associated with reflector slope populations; note inverted color bar. All gridded at 0.25° × 0.25°. Data sets (Figures 3b and 3c) are produced using a single mean value from each individual flight segment. A 50 km radius median filter is applied during this collation process. If there are insufficient data, here defined as less than three values available within 50 km of the center of the grid point, no value is allocated to the gridded data set.

4. Conclusions

On the regional scale, observations of continuous englacial reflectors have been accurately digitized from RES data by hand, and the results successfully used to investigate regional changes in ice flow [*Siegert et al.*, 2004; *Rippin et al.*, 2006], and directly in ice flow modeling studies [e.g., *Conway et al.*, 1999; *Siegert et al.*, 2003; *Martín et al.*, 2006; *Waddington et al.*, 2007; *Eisen*, 2008; *Martín et al.*, 2009]. However, a rapid increase in the amount of RES observations from Greenland and Antarctica mean that successful automatic RES algorithms that allow the extraction of isochrone data may now also be of use to the glaciological and paleoclimate communities.

Here we find that ARESP and the continuity index can both be used to automatically identify regions of traceable isochronous reflectors. By developing and using ARESP, we estimate the proportion of isochronous data here. The method developed measures the proportion of RES data which contains isochronous reflectors by automatically assessing the number of measurable reflectors and the local variance of reflector slope. We find that measurable isochronous reflectors occur most frequently between 1000 and 3000 m in depth, and across about 36% of the data (by flight location), and about 41% of the total number of data. The occurrence of isochronous reflectors is mainly independent of the year the CReSIS radar system was flown, though measurements from the P3-platform have tended to yield data which are more amenable to additional forms of automated measurement.

Regions with lower continuity index, or featuring a low ARESP-estimated proportion of isochronous reflectors, are most likely to be coastal regions experiencing faster flow. Faster flow tends to result in disrupted reflectors, the coastal regions also tend to feature shallow ice, both of which can lead to a lack of measurable isochronous reflectors. Central northeastern regions contain large volumes of ice from cold glacial periods. This results in fewer measurable isochronous reflectors, likely because the high concentration of carbonate

dust in cold and windy climates has neutralized layers of volcanically derived acids that may otherwise cause radar returns [*Jacobel and Hodge*, 1995]. These results have implications for the use of automatically measured isochronous data in evaluating ice sheet models. For Greenland, there may be only rather limited isochrone data available from faster-flowing coastal regions. There will also be less information available from regions that contain large volumes of cold glacial period ice. These data limitations will be the fundamental constraint on automated three-dimensional age field generation, and likewise the use of RES observations for the evaluation of models of Greenland ice flow.

Acknowledgments

The work was funded by NERC grant NE/J004804/1 and also forms part of the British Antarctic Survey Polar Science for Planet Earth Programme. Computations were undertaken on the BAS SciHub computing cluster, for which we thank NERC national capability funding. We acknowledge the use of data products from CReSIS generated with support from NSF grant ANT-0424589 and NASA Operation IceBridge grant NNX10AT68G. Code used to perform the calculations can be obtained from the first author. Data are publicly available at https://data.cresis.ku.edu/data/rds/. The authors gratefully acknowledge valuable input from two anonymous referees.

The Editor thanks Gwendolyn Leysinger Vieli for her assistance in evaluating this paper.

References

Bell, R. E., et al. (2011), Widespread persistent thickening of the East Antarctic ice sheet by freezing from the base, *Science*, *331*, 1592–1595.

Bogorodsky, V. V., C. R. Bentley, and P. E. Gudmandsen (1985), *Radioglaciology: Glaciology and Quaternary Geology*, Springer, Netherlands.

Clarke, G., N. Lhomme, and S. Marshall (2005), Tracer transport in the Greenland ice sheet: Three-dimensional isotopic stratigraphy, *Quat. Sci. Rev.*, *24*, 155–171.

Conway, H., B. L. Hall, G. H. Denton, A. M. Gades, and E. D. Waddington (1999), Past and future grounding-line retreat of the West Antarctic Ice Sheet, *Science*, *286*, 280–283.

Eisen, O. (2008), Inference of velocity pattern from isochronous layers in firn, using an inverse method, *J. Glaciol.*, *54*, 613–630.

Fahnestock, M., W. Abdalati, S. Luo, and S. Gogineni (2001), Internal layer tracing and age-depth-accumulation relationships for the northern Greenland ice sheet, *J. Geophys. Res.*, *106*, 33,789–33,797, doi:10.1029/2001JD900200.

Gogineni, S., D. Tammana, D. Braaten, C. Leuschen, T. Akins, J. Legarsky, P. Kanagaratnam, J. Stiles, C. Allen, and K. Jezek (2001), Coherent radar ice thickness measurements over the Greenland ice sheet, *J. Geophys. Res.*, *106*, 33,761–33,772, doi:10.1029/2001JD900183.

Gogineni, S., et al. (2007), Polar radar for ice sheet measurements (prism), *Remote Sens. Environ.*, *111*, 204–211.

Gogineni, S. P. (2012), CReSIS RDSData with digital data, Lawrence, Kans., http://data.cresis.ku.edu/.

Heimbach, P., and V. Bugnion (2009), Greenland ice-sheet volume sensitivity to basal, surface and initial conditions derived from an adjoint model, *Ann. Glaciol.*, *50*, 67–80.

Hindmarsh, R., G.-M. Leysinger Vieli, and F. Parrenin (2009), A large-scale numerical model for computing isochrone geometry, *Ann. Glaciol.*, *50*, 130–140.

Intergovernmental Panel on Climate Change (2013), Climate change 2013: The physical science basis, in *Contribution of Working Group I to the Fifth Assessment Report of the Intergovernmental Panel on Climate Change*, edited by T. F. Stocker et al., Cambridge Univ. Press, Cambridge, U. K. and New York.

Jacobel, R. W., and S. M. Hodge (1995), Radar internal layers from the Greenland summit, *Geophys. Res. Lett.*, *22*, 587–590.

Joughin, I., B. E. Smith, I. M. Howat, T. Scambos, and T. Moon (2010), Greenland flow variability from ice-sheet-wide velocity mapping, *J. Glaciol.*, *56*, 415–430.

Karlsson, N. B., D. M. Rippin, R. G. Bingham, and D. G. Vaughan (2012), A 'continuity-index' for assessing ice-sheet dynamics from radar-sounded internal layers, *Earth Planet. Sci. Lett.*, *335-336*, 88–94.

Karlsson, N. B., D. Dahl-Jensen, S. P. Gogineni, and J. D. Paden (2013), Tracing the depth of the Holocene ice in North Greenland from radio-echo sounding data, *Ann. Glaciol.*, *54*, 44–50.

Leysinger Vieli, G. J. M. C., R. C. A. Hindmarsh, and M. J. Siegert (2007), Three-dimensional flow influences on radar layer stratigraphy, *Ann. Glaciol.*, *46*, 22–28.

Leysinger Vieli, G. J.-M. C., R. C. A. Hindmarsh, M. J. Siegert, and S. Bo (2011), Time-dependence of the spatial pattern of accumulation rate in East Antarctica deduced from isochronic radar layers using a 3-D numerical ice flow model, *J. Geophys. Res.*, *116*, F02018, doi:10.1029/2010JF001785.

Lhomme, N., G. Clarke, and S. Marshall (2005), Tracer transport in the Greenland Ice Sheet: Constraints on ice cores and glacial history, *Quat. Sci. Rev.*, *24*, 173–194.

Lohoefener, A. (2006), Design and development of a multi-channel radar depth sounder, CReSIS Technical Report, Univ. of Kansas.

Martín, C., R. C. A. Hindmarsh, and F. J. Navarro (2006), Dating ice flow change near the flow divide at Roosevelt Island, Antarctica, by using a thermomechanical model to predict radar stratigraphy, *J. Geophys. Res.*, *111*, F01011, doi:10.1029/2005JF000326.

Martín, C., G. H. Gudmundsson, H. D. Pritchard, and O. Gagliardini (2009), On the effects of anisotropic rheology on ice flow, internal structure, and the age-depth relationship at ice divides, *J. Geophys. Res.*, *114*, F04001, doi:10.1029/2008JF001204.

Matsuoka, K., A. Conway, G. Catania, and C. Raymond (2009), Radar signatures beneath a surface topographic lineation near the outlet of Kamb Ice Stream and Engelhardt Ice Ridge, West Antarctica, *Ann. Glaciol.*, *50*, 98–104.

Namburi, S. P. V. (2003), Design and development of an advanced coherent radar depth sounder, Master's thesis, Department of Electrical Engineering and Computer Science, Univ. of Kansas.

Namburi, S. P. V. (2007), Design and development of an advanced coherent radar depth sounder, *Tech. Rep. 115*, CReSIS Technical Report, University of Kansas.

Oswald, G. K. A., and S. P. Gogineni (2008), Recovery of subglacial water extent from Greenland radar survey data, *J. Glaciol.*, *54*, 94–106.

Rippin, D. M., M. J. Siegert, J. L. Bamber, D. G. Vaughan, and H. F. J. Corr (2006), Switch-off of a major enhanced ice flow unit in East Antarctica, *Geophys. Res. Lett.*, *33*, L15501, doi:10.1029/2006GL026648.

Siegert, M., R. Hindmarsh, and G. Hamilton (2003), Evidence for a large surface ablation zone in central East Antarctica during the last Ice Age, *Quat. Res.*, *59*, 114–121.

Siegert, M. J., et al. (2004), Ice flow direction change in interior West Antarctica, *Science*, *305*, 1948–1951.

Sime, L., R. Hindmarsh, and H. Corr (2011), Automated processing to derive dip angles of englacial radar reflectors in ice sheets, *J. Glaciol.*, *57*, 260–266.

Sime, L. C., and R. I. Ferguson (2003), Information on grain sizes in Gravel-Bed Rivers by automated image analysis, *J. Sediment. Res.*, *73*, 630–636.

Velicogna, I. (2009), Increasing rates of ice mass loss from the Greenland and Antarctic ice sheets revealed by GRACE, *Geophys. Res. Lett.*, *36*, L19503, doi:10.1029/2009GL040222.

Waddington, E. D., T. A. Neumann, M. R. Koutnik, H.-P. Marshall, and D. L. Morse (2007), Inference of accumulation-rate patterns from deep layers in glaciers and ice sheets, *Int. Glaciol. Soc.*, *53*, 694–712.